J|A|C|S ARTICLES

Published on Web 03/09/2009

Controlled Self-Assembly of C_3-Symmetric Hexa-*peri*-hexabenzocoronenes with Alternating Hydrophilic and Hydrophobic Substituents in Solution, in the Bulk, and on a Surface

Xinliang Feng,[†] Wojciech Pisula,[†,||] Tibor Kudernac,[‡] Dongqing Wu,[†] Linjie Zhi,[†,§] Steven De Feyter,[‡] and Klaus Müllen*[,†]

Max Planck Institute for Polymer Research, Ackermannweg 10, 55128 Mainz, Germany, Department of Chemistry, Division of Molecular and Nanomaterials, Laboratory of Photochemistry and Spectroscopy, and Institute of Nanoscale Physics and Chemistry, Katholieke Universiteit Leuven (KULeuven), Celestijnenlaan 200 F, B-3001 Leuven, Belgium, and National Center for Nanoscience and Technology of China, Zhongguancun, Beiyitiao 11, 100190 Beijing, P. R. China

Received November 17, 2008; E-mail: muellen@mpip-mainz.mpg.de

Abstract: In this work, we introduce a class of C_3-symmetric hexa-*peri*-hexabenzocoronenes (HBCs) **1** with alternating hydrophilic and hydrophobic substituents to achieve control over the self-assembly of discotic nanographene molecules. Our studies show that the following structural parameters and experimental conditions are essential for tailoring the formation of the liquid-crystalline phase in the bulk as well as the self-assembly in solution and on surfaces: (1) steric demand of alkyl and alkylphenyl substituents; (2) noncovalent hydrophilic−hydrophobic interactions of the substituents; and (3) processing conditions, such as the type and mixture of solvents of different polarities along with the nature of the surface. The substitution of HBC with linear alkyl side chains possessing less steric demand (**1b**) leads to high crystallinity in the bulk solid state and at the liquid−solid interface, and the additional feature of alternating hydrophilic and hydrophobic substituents promotes a high aggregation tendency in polar/apolar solvent mixtures. In contrast, bulky branched alkyl chains (**1a**) and alkylphenyl substituents (**1c**) induce liquid crystallinity over the whole temperature range measured. While **1a** does not show pronounced self-assembly in solution, compound **1c** displays, even at high temperatures, aggregation in polar/apolar solution due to the intermolecular "locking" of peripheral phenyl groups. After solution deposition on a surface, distinct fiber formation is observed for the HBC derivatives, which is related to the solution self-assembly behavior. The present work provides further insight into the molecular design and self-assembly of discotic nanographene materials.

Introduction

In recent years, great scientific and technological efforts have been devoted to molecular columnar structures, mainly because of their potential applications in electronic devices.[1−5] In particular, discotic liquid crystals are of interest in supramolecular chemistry because of their ability to form one-dimensional columnar stacks as a result of their distinct self-organization propensity via π interactions and local phase separation between the flat rigid aromatic cores and flexible peripheral substituents.[6−8] As the building blocks of 2D graphene sheets, hexa-*peri*-hexabenzocoronenes (HBCs) with nanometer size belong to the most studied discotic nanographene species because of the pronounced stability of their columnar mesophases and their high local one-dimensional charge-carrier mobilities.[9−11] These systems[3,12−16] offer a great opportunity

[†] Max Planck Institute for Polymer Research.
[‡] Katholieke Universiteit Leuven.
[§] National Center for Nanoscience and Technology of China.
[||] Present address: Evonik Degussa GmbH, Process Technology & Engineering, Process Technology - New Processes, Rodenbacher Chaussee 4, 63457 Hanau-Wolfgang, Germany.

(1) Schmidt-Mende, L.; Fechtenkotter, A.; Müllen, K.; Moons, E.; Friend, R. H.; MacKenzie, J. D. *Science* **2001**, *293*, 1119–1122.
(2) Pisula, W.; Menon, A.; Stepputat, M.; Lieberwirth, I.; Kolb, U.; Tracz, A.; Sirringhaus, H.; Pakula, T.; Müllen, K. *Adv. Mater.* **2005**, *17*, 684–689.
(3) Xiao, S. X.; Tang, J. Y.; Beetz, T.; Guo, X. F.; Tremblay, N.; Siegrist, T.; Zhu, Y. M.; Steigerwald, M.; Nuckolls, C. *J. Am. Chem. Soc.* **2006**, *128*, 10700–10701.
(4) Wu, J. S.; Pisula, W.; Müllen, K. *Chem. Rev.* **2007**, *107*, 718–747.
(5) Feng, X. L.; Liu, M. Y.; Pisula, W.; Takase, M.; Li, J. L.; Müllen, K. *Adv. Mater.* **2008**, *20*, 2684–2689.
(6) Sergeyev, S.; Pisula, W.; Geerts, Y. H. *Chem. Soc. Rev.* **2007**, *36*, 1902–1929.
(7) Laschat, S.; Baro, A.; Steinke, N.; Giesselmann, F.; Hagele, C.; Scalia, G.; Judele, R.; Kapatsina, E.; Sauer, S.; Schreivogel, A.; Tosoni, M. *Angew. Chem., Int. Ed.* **2007**, *46*, 4832–4887.
(8) Kumar, S. *Chem. Soc. Rev.* **2006**, *35*, 83–109.
(9) Debije, M. G.; Piris, J.; de Haas, M. P.; Warman, J. M.; Tomovic, Z.; Simpson, C. D.; Watson, M. D.; Müllen, K. *J. Am. Chem. Soc.* **2004**, *126*, 4641–4645.
(10) Watson, M. D.; Fechtenkotter, A.; Müllen, K. *Chem. Rev.* **2001**, *101*, 1267–1300.
(11) van de Craats, A. M.; Warman, J. M.; Fechtenkotter, A.; Brand, J. D.; Harbison, M. A.; Müllen, K. *Adv. Mater.* **1999**, *11*, 1469–1472.
(12) Palma, M.; Levin, J.; Lemaur, V.; Liscio, A.; Palermo, V.; Cornil, J.; Geerts, Y.; Lehmann, M.; Samori, P. *Adv. Mater.* **2006**, *18*, 3313–3317.

to tailor the chemical structures and physical properties of the established nanoscopic objects,[17−31] in contrast to the well-known carbon nanotubes,[32−38] graphene nanoribbons,[39] and nanowires of inorganic semiconductors.[40−44]

The growth of long fibrous nanostructures from alkylated HBCs depends on the nature of the molecules, where π-stacking interactions compete with intermolecular van der Waals interactions during solution self-assembly and deposition on the surface.[45−47] In contrast, HBCs with amphiphilic character are particularly interesting for the fabrication of different functional nanostructures on the surfaces, which has triggered enormous interest in the recent several years.[13,15,48−51] Among them, Aida and co-workers demonstrated that amphiphilic-type substituents were essential to roll-up HBCs into outstanding tubular nanostructures.[13,15,48,49] Intracolumnar packing of triangle-shaped discotics in the bulk state was controlled by an alternating substitution of hydrophilic and hydrophobic substituents, which served as additional driving force for the local phase separation to induce a helical organization with a specific pitch and high charge-carrier transport.[52] In this sense, a delicate balance between the different segments of the molecular building blocks is required. The organization of other HBCs and π-conjugated molecules in the literature indicate that besides the intrinsic nature of the molecular shape and symmetry, several other structural parameters and experimental conditions are essential for controlling the supramolecular arrangement and phase formation: (1) the steric demand of the substituents; (2) noncovalent forces, such as π-stacking, hydrogen-bonding, dipole, and hydrophilic−hydrophobic interactions; and (3) the processing methods, the type of solvent, and the nature of the surface.[20,53,54]

Over the past decade, the supramolecular chemistry of a variety of HBC derivatives with different substitutional symmetries and peripheral decorations has been widely investigated.[15,45,50,51,55,56] However, C_3-symmetric discotics, which are appealing for organization,[21,57,58] still are among the less investigated species in the nanographene systems.[59−61] In this work, we present a new class of C_3-symmetric HBCs with alternating hydrophilic (trieth-

(13) Yamamoto, Y.; Fukushima, T.; Suna, Y.; Ishii, N.; Saeki, A.; Seki, S.; Tagawa, S.; Taniguchi, M.; Kawai, T.; Aida, T. *Science* **2006**, *314*, 1761–1764.
(14) Palermo, V.; Morelli, S.; Simpson, C.; Müllen, K.; Samori, P. *J. Mater. Chem.* **2006**, *16*, 266–271.
(15) Hill, J. P.; Jin, W. S.; Kosaka, A.; Fukushima, T.; Ichihara, H.; Shimomura, T.; Ito, K.; Hashizume, T.; Ishii, N.; Aida, T. *Science* **2004**, *304*, 1481–1483.
(16) Palermo, V.; Samori, P. *Angew. Chem., Int. Ed.* **2007**, *46*, 4428–4432.
(17) Ajayaghosh, A.; Praveen, V. K. *Acc. Chem. Res.* **2007**, *40*, 644–656.
(18) Ajayaghosh, A.; Varghese, R.; Praveen, V. K.; Mahesh, S. *Angew. Chem., Int. Ed.* **2006**, *45*, 3261–3264.
(19) Ajayaghosh, A.; Varghese, R.; Mahesh, S.; Praveen, V. K. *Angew. Chem., Int. Ed.* **2006**, *45*, 7729–7732.
(20) Jonkheijm, P.; Hoeben, F. J. M.; Kleppinger, R.; van Herrikhuyzen, J.; Schenning, A.; Meijer, E. W. *J. Am. Chem. Soc.* **2003**, *125*, 15941–15949.
(21) van Gorp, J. J.; Vekemans, J.; Meijer, E. W. *J. Am. Chem. Soc.* **2002**, *124*, 14759–14769.
(22) Schenning, A.; Jonkheijm, P.; Peeters, E.; Meijer, E. W. *J. Am. Chem. Soc.* **2001**, *123*, 409–416.
(23) Ajayaghosh, A.; George, S. J. *J. Am. Chem. Soc.* **2001**, *123*, 5148–5149.
(24) El-Ghayoury, A.; Schenning, A.; van Hal, P. A.; van Duren, J. K. J.; Janssen, R. A. J.; Meijer, E. W. *Angew. Chem., Int. Ed.* **2001**, *40*, 3660–3663.
(25) Jonkheijm, P.; Miura, A.; Zdanowska, M.; Hoeben, F. J. M.; De Feyter, S.; Schenning, A.; De Schryver, F. C.; Meijer, E. W. *Angew. Chem., Int. Ed.* **2004**, *43*, 74–78.
(26) Schenning, A.; Meijer, E. W. *Chem. Commun.* **2005**, 3245–3258.
(27) Jonkheijm, P.; Stutzmann, N.; Chen, Z. J.; de Leeuw, D. M.; Meijer, E. W.; Schenning, A.; Wurthner, F. *J. Am. Chem. Soc.* **2006**, *128*, 9535–9540.
(28) Percec, V.; Aqad, E.; Peterca, M.; Rudick, J. G.; Lemon, L.; Ronda, J. C.; De, B. B.; Heiney, P. A.; Meijer, E. W. *J. Am. Chem. Soc.* **2006**, *128*, 16365–16372.
(29) Wu, D. Q.; Zhi, L. J.; Bodwell, G. J.; Cui, G. L.; Tsao, N.; Müllen, K. *Angew. Chem., Int. Ed.* **2007**, *46*, 5417–5420.
(30) Ajayaghosh, A.; Vijayakumar, C.; Praveen, V. K.; Babu, S. S.; Varghese, R. *J. Am. Chem. Soc.* **2006**, *128*, 7174–7175.
(31) Ajayaghosh, A.; Praveen, V. K.; Varghese, R. *Adv. Mater.* **2007**, *19*, 411–415.
(32) Zhang, Z. Y.; Liang, X. L.; Wang, S.; Yao, K.; Hu, Y. F.; Zhu, Y. Z.; Chen, Q.; Zhou, W. W.; Li, Y.; Yao, Y. G.; Zhang, J.; Peng, L. M. *Nano Lett.* **2007**, *7*, 3603–3607.
(33) Avouris, P.; Chen, Z. H.; Perebeinos, V. *Nat. Nanotechnol.* **2007**, *2*, 605–615.
(34) Kang, S. J.; Kocabas, C.; Ozel, T.; Shim, M.; Pimparkar, N.; Alam, M. A.; Rotkin, S. V.; Rogers, J. A. *Nat. Nanotechnol.* **2007**, *2*, 230–236.
(35) Tseng, Y. C.; Phoa, K.; Carlton, D.; Bokor, J. *Nano Lett.* **2006**, *6*, 1364–1368.
(36) Regan, B. C.; Aloni, S.; Ritchie, R. O.; Dahmen, U.; Zettl, A. *Nature* **2004**, *428*, 924–927.
(37) Baughman, R. H.; Zakhidov, A. A.; de Heer, W. A. *Science* **2002**, *297*, 787–792.
(38) Tans, S. J.; Verschueren, A. R. M.; Dekker, C. *Nature* **1998**, *393*, 49–52.
(39) Li, X. L.; Wang, X. R.; Zhang, L.; Lee, S. W.; Dai, H. J. *Science* **2008**, *319*, 1229–1232.
(40) Ma, R. M.; Dai, L.; Huo, H. B.; Xu, W. J.; Oin, G. G. *Nano Lett.* **2007**, *7*, 3300–3304.
(41) Xiang, J.; Lu, W.; Hu, Y. J.; Wu, Y.; Yan, H.; Lieber, C. M. *Nature* **2006**, *441*, 489–493.
(42) Ng, H. T.; Han, J.; Yamada, T.; Nguyen, P.; Chen, Y. P.; Meyyappan, M. *Nano Lett.* **2004**, *4*, 1247–1252.
(43) Duan, X. F.; Niu, C. M.; Sahi, V.; Chen, J.; Parce, J. W.; Empedocles, S.; Goldman, J. L. *Nature* **2003**, *425*, 274–278.
(44) Xia, Y. N.; Yang, P. D.; Sun, Y. G.; Wu, Y. Y.; Mayers, B.; Gates, B.; Yin, Y. D.; Kim, F.; Yan, Y. Q. *Adv. Mater.* **2003**, *15*, 353–389.
(45) Kastler, M.; Pisula, W.; Wasserfallen, D.; Pakula, T.; Müllen, K. *J. Am. Chem. Soc.* **2005**, *127*, 4286–4296.
(46) Wu, J. S.; Watson, M. D.; Zhang, L.; Wang, Z. H.; Müllen, K. *J. Am. Chem. Soc.* **2004**, *126*, 177–186.
(47) Feng, X. L.; Pisula, W.; Takase, M.; Dou, X.; Enkelmann, V.; Wagner, M.; Ding, N.; Müllen, K. *Chem. Mater.* **2008**, *20*, 2872–2874.
(48) Yamamoto, T.; Fukushima, T.; Yamamoto, Y.; Kosaka, A.; Jin, W.; Ishii, N.; Aida, T. *J. Am. Chem. Soc.* **2006**, *128*, 14337–14340.
(49) Jin, W.; Fukushima, T.; Niki, M.; Kosaka, A.; Ishii, N.; Aida, T. *Proc. Natl. Acad. Sci. U.S.A.* **2005**, *102*, 10801–10806.
(50) Lee, M.; Kim, J. W.; Peleshanko, S.; Larson, K.; Yoo, Y. S.; Vaknin, D.; Markutsya, S.; Tsukruk, V. V. *J. Am. Chem. Soc.* **2002**, *124*, 9121–9128.
(51) Wu, J. S.; Li, J. X.; Kolb, U.; Müllen, K. *Chem. Commun.* **2006**, 48–50.
(52) Feng, X.; Marcon, V.; Pisula, W.; Kirkpatrick, J.; Grozema, F.; Andrienko, D.; Kremer, K.; Müllen, K. *Nat. Mater.* **2009**, under revision.
(53) van Hameren, R.; Schon, P.; van Buul, A. M.; Hoogboom, J.; Lazarenko, S. V.; Gerritsen, J. W.; Engelkamp, H.; Christianen, P. C. M.; Heus, H. A.; Maan, J. C.; Rasing, T.; Speller, S.; Rowan, A. E.; Elemans, J.; Nolte, R. J. M. *Science* **2006**, *314*, 1433–1436.
(54) van Hameren, R.; van Buul, A. M.; Castriciano, M. A.; Villari, V.; Micali, N.; Schon, P.; Speller, S.; Scolaro, L. M.; Rowan, A. E.; Elemans, J.; Nolte, R. J. M. *Nano Lett.* **2008**, *8*, 253–259.
(55) Wu, J. S.; Fechtenkotter, A.; Gauss, J.; Watson, M. D.; Kastler, M.; Fechtenkotter, C.; Wagner, M.; Müllen, K. *J. Am. Chem. Soc.* **2004**, *126*, 11311–11321.
(56) Feng, X.; Pisula, W.; Müllen, K. *J. Am. Chem. Soc.* **2007**, *129*, 14116–14117.
(57) Smulders, M. M. J.; Schenning, A.; Meijer, E. W. *J. Am. Chem. Soc.* **2008**, *130*, 606–611.
(58) Furukawa, S.; Uji-i, H.; Tahara, K.; Ichikawa, T.; Sonoda, M.; De Schryver, F. C.; Tobe, Y.; De Feyter, S. *J. Am. Chem. Soc.* **2006**, *128*, 3502–3503.
(59) Feng, X. L.; Wu, J. S.; Ai, M.; Pisula, W.; Zhi, L. J.; Rabe, J. P.; Müllen, K. *Angew. Chem., Int. Ed.* **2007**, *46*, 3033–3036.
(60) Feng, X. L.; Wu, J. S.; Enkelmann, V.; Müllen, K. *Org. Lett.* **2006**, *8*, 1145–1148.
(61) Feng, X. L.; Pisula, W.; Ai, M.; Groper, S.; Rabe, J. P.; Müllen, K. *Chem. Mater.* **2008**, *20*, 1191–1193.

Chart 1. C_3-Symmetric HBC Derivatives with Alternating Hydrophilic and Hydrophobic Substituents

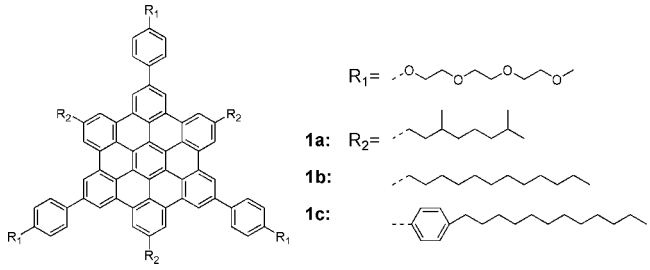

Scheme 1. General Synthetic Route to **1**[a]

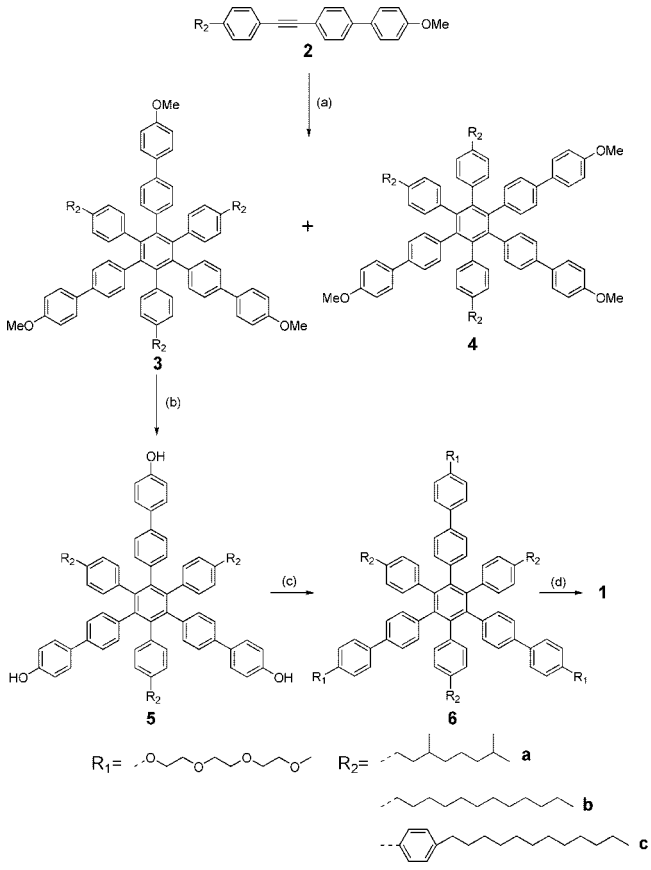

[a] (a) $Co_2(CO)_8$, dioxane, reflux; (b) BBr_3, CH_2Cl_2, 0 °C to RT; (c) (4-toluenesulfonyl)triethylene glycol monomethyl ether, DMF, KOH, 80 °C; (d) $FeCl_3$, CH_3NO_2, CH_2Cl_2, 75−90%.

ylene glycol) and hydrophobic (alkyl or alkylphenyl) substituents (compounds **1**, Chart 1). They incorporate the key structural parameters, such as different steric demands of the substituents and noncovalent hydrophilic−hydrophobic interactions, that enable control over the self-assembly in the bulk, in solution, at the liquid−solid interface, and on surfaces.

Results and Discussion

Synthesis. As shown in Scheme 1, the synthesis of C_3-symmetric discotic HBCs **1** started from asymmetric diphenylacetylene derivatives **2**, which were easily available via Sonogashira coupling reactions (see the Supporting Information). Subsequent cyclotrimerization of these molecules in dioxane catalyzed by $Co_2(CO)_8$ gave a series of C_3-symmetric hexaphenylbenzene derivatives **3** as well as their asymmetric analogues **4**. The two isomers **3** and **4** (with a ratio of ∼1:2), which have different polarities, could easily be separated by column chromatography. Subsequent BBr_3-mediated demethylation of **3** under mild conditions gave compounds **5** in high yields, which were further reacted with (4-toluenesulfonyl)triethylene glycol monomethyl ether in DMF at 80 °C in the presence of a base to yield precursors **6**. Oxidative cyclodehydrogenation of **6** with $FeCl_3$ resulted in the C_3-symmetric discotic HBCs **1** as yellow powders in good yields. All of the compounds were soluble in CH_2Cl_2, THF, and toluene, thus allowing further purification by column chromatography (silica gel, CH_2Cl_2/MeOH).

The final products were characterized by MALDI-TOF MS spectrometry, ^1H and ^{13}C NMR spectroscopy, and elemental analysis and were shown to be in full agreement with the desired structures (see the Supporting Information).

Self-Assembly in Bulk. The thermal properties of compounds **1a**−**c** were determined by differential scanning calorimetry (DSC). The DSC scan for **1a** showed a phase transition at 14 °C with an enthalpy of 1.4 J/g, while that for **1b** revealed a transition at 74 °C with a larger enthalpy of 40.9 J/g. In contrast, compound **1c** did not have any phase transitions within the investigated temperature range.

The supramolecular organization of these three molecules was studied by two-dimensional wide-angle X-ray scattering (2D-WAXS). For these measurements, macroscopically oriented specimens were prepared by filament extrusion.[62] Because of their plasticity under ambient conditions, samples of **1a** and **1c** were extruded at 25 °C, while **1b** was prepared above the observed phase transition temperature at 100 °C.

A typical liquid-crystalline (LC) hexagonal columnar phase was observed for all three compounds, as indicated by the characteristic 2D-WAXS patterns (Figure 1). Compounds **1a** and **1c** revealed an LC phase over the whole temperature range between −100 °C and 200 °C, while **1b** reached this phase at 74 °C. Typically, in this phase the columns are arranged hexagonally with respect to each other, as implied by the positions of the equatorial reflections at a ratio of $1:\sqrt{3}:2$. In the present case, the 2D lateral unit cell parameters varied depending on the chemical design of the derivatives (as summarized in Table 1). The meridional reflections were attributed to a π-stacking spacing of 0.35 nm between the disk-shaped molecules, and thus, the discs were packed with their planes perpendicular to the columnar axis. Previously reported solid-state NMR experiments on alkylated HBCs revealed a lateral rotation of the molecules and a pronounced motion of the alkyl side chains in the LC phase, resulting in the appearance of an amorphous halo in the pattern,[63] which was also observed in our case. In contrast to **1a** and **1c**, the pattern of compound **1b** pointed toward a more ordered crystalline phase below 74 °C with a typical herringbone arrangement (Figure 1b). A tilting angle of ∼30° for the molecules with respect to the columnar axis was derived from the off-meridional scattering intensities.

The formation of a crystalline phase clearly distinguished **1b** from **1a** and **1c**, both of which showed an LC phase over the whole temperature range investigated. This clear difference could be explained in terms of the steric demand of the alkyl substituents. Since dodecyl side chains are less sterically demanding, **1b** can adopt a well-organized crystalline phase

(62) Pisula, W.; Tomovic, Z.; Simpson, C.; Kastler, M.; Pakula, T.; Müllen, K. *Chem. Mater.* **2005**, *17*, 4296–4303.
(63) Pisula, W.; Kastler, M.; Wasserfallen, D.; Mondeshki, M.; Piris, J.; Schnell, I.; Müllen, K. *Chem. Mater.* **2006**, *18*, 3634–3640.

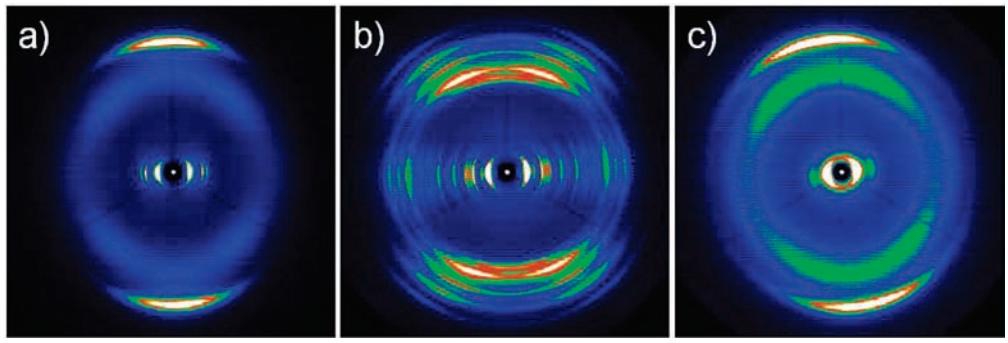

Figure 1. 2D-WAXS of **1b** at (a) 130 °C and (b) at 30 °C (after annealing) and (c) of **1c** at 30 °C.

Table 1. Packing Parameters of Compounds **1** in Their Corresponding Phases, As Derived from 2D-WAXS

		intracolumnar packing		
compound	phase	a_{hex} (nm)[a]	$d_{\pi\text{-stacking}}$ (nm)[b]	tilt angle (deg)
1a	liquid crystalline	2.85	0.35	0
1b	crystalline	n.a.	0.35	30
	liquid crystalline	3.06	0.36	0
1c	liquid crystalline	3.28	0.35	0

[a] a_{hex} = hexagonal unit cell parameter; n.a. = not assigned. [b] $d_{\pi\text{-stacking}}$ = π-stacking spacing.

under ambient conditions. This is not the case for **1a** because of the branched alkyl chains, which are more bulky and thus disturb the molecular π interactions, resulting in the less ordered LC phase. This is in line with the good solubility and poor aggregation behavior of **1a** in solution, as described in the next sections. The introduction of additional phenyl groups in **1c** had a similar effect on the formation of the LC state at low temperature because of the increase in the steric influence in the disk periphery. The molecular design of **1c** with its hexaphenyl substitution can lead to an interlocking of the molecules and thus a better organization.[64,65] While this is not obvious from the X-ray scattering data for **1c** in the bulk, it can be discerned from the behavior in solution (see the next section). Finally, it has to be noted that the structural analysis did not indicate an apparent influence of the alternating hydrophilic/hydrophobic substitution on the bulk organization. However, this is in stark contrast to the strong effect on fiber formation from solvent mixtures, which will be presented below.

Self-Assembly in Solution. The spontaneous formation of molecular assemblies via π interactions in solution or the condensed state is a characteristic feature of alkyl- and alkylphenyl-substituted HBCs. Electronic and ^{1}H NMR spectroscopies provide a sensitive probe of these interactions.[45] UV−vis and photoluminescence spectra were first recorded for **1** in $CHCl_3$ at 1×10^{-5} M (Figure 2 and Figures S2 and S3 in the Supporting Information). Compounds **1a** and **1b** revealed essentially similar UV−vis spectra, with band maxima at 370 nm (β band) and 400 nm (p band) and an emission maximum at 498 nm. In contrast, compound **1c** showed the absorption bands at 375 nm (β band) and 418 nm (p band), which were red-shifted with respect to **1a** and **1b** because of the three additional phenyl groups at the periphery of the corona. As has been observed for other hexaphenyl-substituted HBCs, the emission of **1c** was structureless.[66]

^{1}H NMR spectra of **1** (8.0×10^{-3} M in $CDCl_2CDCl_2$) were recorded over a temperature range of 25−140 °C. Two kinds of core protons were clearly recognized at room temperature for **1a** and **1b**, corresponding to the neighboring corona protons with alkyl and phenyl substitutions, whereas under these conditions, **1c** revealed significant line broadening and shielding due to possible interlocking of pendant phenyl rings and π interactions (Figure S1 in the Supporting Information). As the temperature was increased from 25 to 140 °C, the HBC core proton signals of **1a** and **1b** experienced a similar downfield shift (~0.35 ppm), which could be ascribed to the decoupling of face-to-face stacking of the disk molecules in solution. Although the spectrum of **1c** was clearly resolved at high temperature, a large downfield shift of the core proton signals as observed for **1a** and **1b** was not detectable, indicating strong intermolecular interactions of **1c** in solution.[67]

Concentration-dependent UV−vis spectra (concentration range from 1×10^{-4} to 1×10^{-7} M) of compounds **1** in $CHCl_3$, THF, and toluene (not shown) revealed only slight differences. It is known that the self-assembly of HBC in solution is sensitive to solvent effects, particularly in highly polar solvents.[45] In view of the hydrophilic and hydrophobic substituents of **1**, a cosolvent system appeared to be attractive for controlling the self-assembly by the induction of microphase separation in polar and apolar environments.[68−71] Therefore, the photophysical properties of **1** (1×10^{-5} M) were studied in the mixture of a polar solvent (methanol) and a less polar solvent (chloroform). As the MeOH/$CHCl_3$ ratio increased, the β-band absorption maximum of **1b** first shifted hypsochromically from 370 to 365 nm as the result of a solvochromic effect, while the intensity of the p band at 400 nm decreased (Figure 2a). A further increase in the MeOH/$CHCl_3$ ratio up to 1:2 led to a significant broadening and tailing of the UV−vis spectrum. On the other hand, increasing the methanol fraction led to remarkably broadened and bathochro-

(64) Fechtenkotter, A.; Saalwachter, K.; Harbison, M. A.; Müllen, K.; Spiess, H. W. *Angew. Chem., Int. Ed.* **1999**, *38*, 3039–3042.
(65) Pisula, W.; Tomovic, Z.; Watson, M. D.; Müllen, K.; Kussmann, J.; Ochsenfeld, C.; Metzroth, T.; Gauss, J. *J. Phys. Chem. B* **2007**, *111*, 7481–7487.
(66) Feng, X. L.; Pisula, W.; Zhi, L. J.; Takase, M.; Müllen, K. *Angew. Chem., Int. Ed.* **2008**, *47*, 1703–1706.
(67) On the basis of the ^{1}H NMR measurements, the strong intermolecular interactions of **1c** in solution are not necessarily related only to π interactions between neighboring HBC molecules; intermolecular interlocking of pendant phenyl groups may play an important role too. This effect further determines the high thermal stability of aggregates formed in the cosolvents as described later in the article.
(68) Ryu, J. H.; Hong, D. J.; Lee, M. *Chem. Commun.* **2008**, 1043–1054.
(69) Tobe, Y.; Utsumi, N.; Kawabata, K.; Nagano, A.; Adachi, K.; Araki, S.; Sonoda, M.; Hirose, K.; Naemura, K. *J. Am. Chem. Soc.* **2002**, *124*, 5350–5364.
(70) Lee, M.; Cho, B. K.; Zin, W. C. *Chem. Rev.* **2001**, *101*, 3869–3892.
(71) Lahiri, S.; Thompson, J. L.; Moore, J. S. *J. Am. Chem. Soc.* **2000**, *122*, 11315–11319.

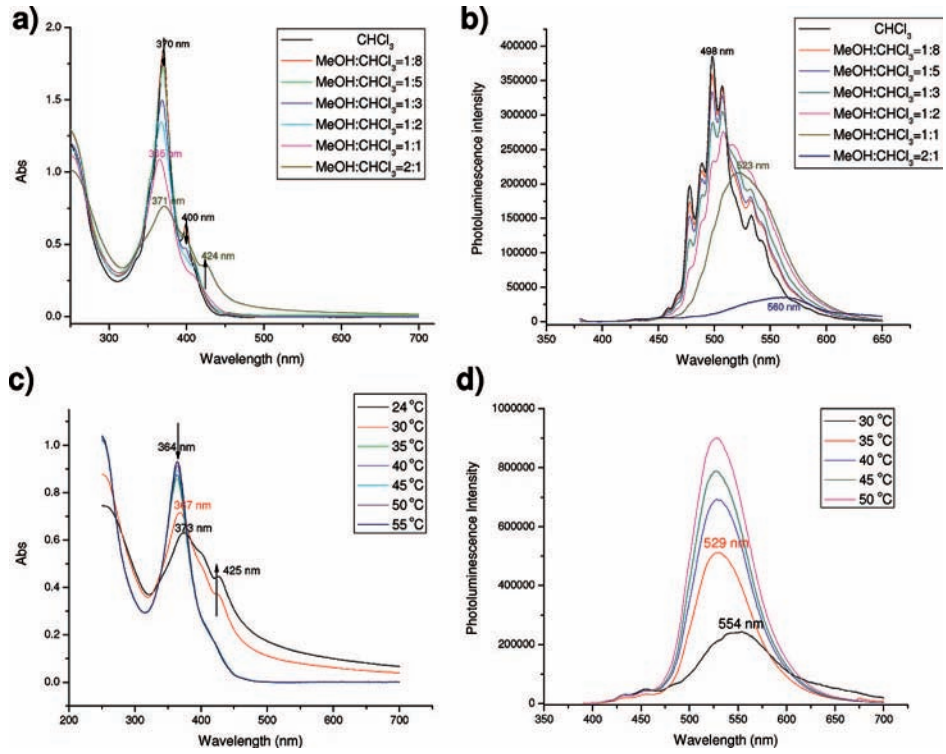

Figure 2. (a) UV−vis and (b) photoluminescence spectra for **1b** in a MeOH/$CHCl_3$ solvent mixture (1.0×10^{-5} M). Variable-temperature (c) UV/vis and (d) photoluminescence spectra of **1b** in 2:1 MeOH/$CHCl_3$ (1.0×10^{-5} M).

mically shifted photoluminescence bands (Figure 2b). The emission maximum was notably shifted from 498 up to 560 nm when the MeOH/$CHCl_3$ ratio reached 2:1, indicating pronounced aggregation under these conditions. Small filaments were slowly formed and began to precipitate after the solution was allowed to stand for several minutes. However, in the case of **1a**, the addition of methanol to the chloroform solution did not result in a bathochromically shifted and broadened spectra or in the precipitation of filaments.[72] Increasing the MeOH/$CHCl_3$ ratio led to a continuous hypsochromic shift of the β band from 370 nm in pure $CHCl_3$ to 361 nm in 5:1 MeOH/$CHCl_3$ (Figure S2a in the Supporting Information), and the photoluminescence spectra turned into a broad, featureless emission band with a peak at 538 nm (from 498 nm in $CHCl_3$, Figure S2b in the Supporting Information), corresponding to a poorer aggregation behavior of **1a** as compared with **1b** in the solvent mixtures.[73] This could be attributed to the branched alkyl chains in **1a**, which suppress intermolecular interactions and thus lead to a better solubility in the solvent mixtures. As for **1b**, a broadened and tailed absorption spectrum was formed for **1c** at a MeOH/$CHCl_3$ ratio of 2:1 (Figure S3a in the Supporting Information). A remarkable aggregation of **1c** was observed in the 3:1 MeOH/$CHCl_3$ solvent mixture, as indicated by the emission maximum at 561 nm. Further standing of the solution led to precipitation of small filaments identical to that seen for **1b**.

UV−vis and photoluminescence spectra were recorded at different temperatures to gain further insight into the reversible self-assembly. In the case of **1b**, a temperature increase from 24 to 35 °C led to a hypsochromical shift of the main bands with an increase of intensity, a narrowing of the broadened absorption spectra, and a disappearance of the tailing (Figure 2c). The original spectra could be recovered by cooling the solution to room temperature. Similarly, the photoluminescence spectra exhibited a prompt transformation at 35 °C with a blue shift of the emission maximum from 554 to 529 nm, implying that aggregates have dissociated at this temperature (Figure 2d). Further temperature increases led only to the display of a band structure with enhanced emission intensity. In contrast, compound **1a** did not reveal any spectral changes within the investigated temperature range (Figure S2c,d in the Supporting Information); the UV/vis and photoluminescence spectra were essentially similar to the disassociated state of **1b**, further indicating the poorer aggregation behavior for **1a.** Surprisingly, no obvious intensity increments in the UV−vis and photoluminescence spectra were observed for compound **1c**, even up to 70 °C (not shown). This suggests that the three additional phenyl groups in **1c** favor intermolecular interactions in solution, leading to high stability of the aggregates, as previously investigated by ^{1}H NMR studies.[74]

The above results revealed pronounced effects of the steric demand of the alkyl substituents of **1** on both the organization in the solid state and the self-assembly in solution. In order to

(72) Similar behavior was also observed for hexaalkyl-substituted HBCs with less sterically demanding substituents (ref 43). These HBCs did not reveal the remarkable bathochromically shifted and broadened absorption and photoluminescence spectra in the cosolvents (7:3 $CHCl_3$/MeOH) because of the lack of intermolecular hydrophilic−hydrophobic interactions. Excess methanol resulted only in formation of precipitates of these HBCs with unstructured morphologies.

(73) The arrangement of the HBC core in the solution aggregates may also affect the spectral features, but in view of the different extents of aggregation in **1a** and **1b** in 2:1 MeOH/$CHCl_3$, this effect will be rather small.

(74) Tomovic, Z.; Van Dongen, J.; George, S. J.; Xu, H.; Pisula, W.; Leclere, P.; Smulders, M. M. J.; De Feyter, S.; Meijer, E. W.; Schenning, A. *J. Am. Chem. Soc.* **2007**, *129*, 16190–16196.

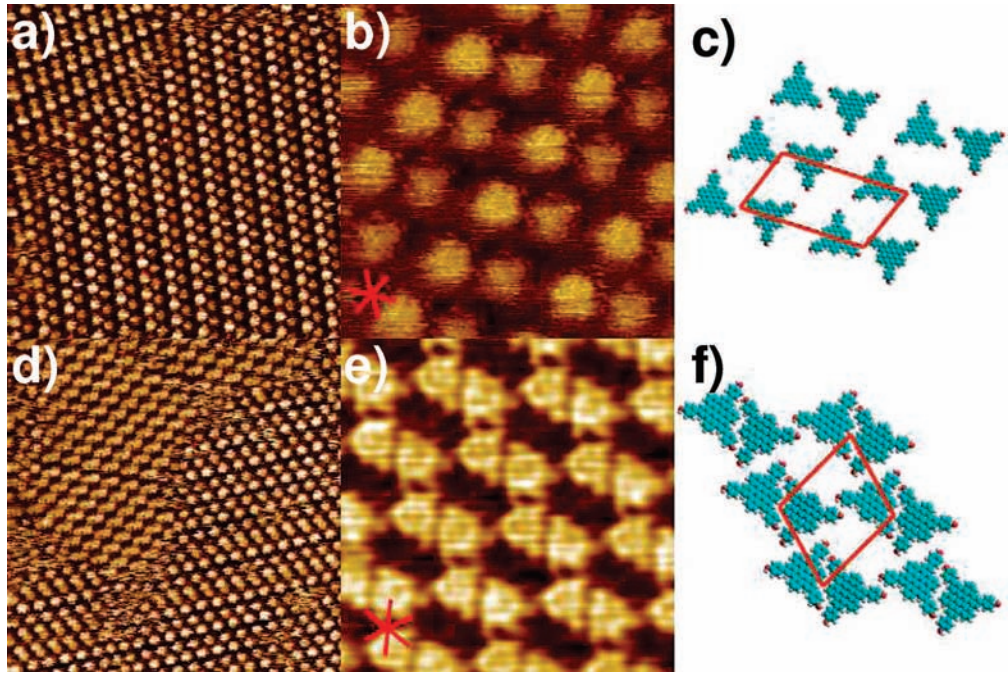

Figure 3. STM images and tentative molecular packing models of **1b** self-assembled at the phenyloctane−graphite interface. (a) STM image of the α-phase (56.5 × 56.5 nm^2, i_T = 21 pA, V_S = −585 mV). (b) High-resolution STM image of the α-phase (13 × 13 nm^2, i_T = 92 pA, V_S = −392 mV). (c) Schematic representation of the tentative packing model of the α-phase, with the unit cell shown. Peripheral side chains have been omitted. (d) STM image of the β-phase (58 × 58 nm^2, i_T = 33 pA, V_S = −669 mV). (e) High-resolution STM image of the β-phase (11.2 × 11.2 nm^2, i_T = 22 pA, V_S = −885 mV). (f) Schematic representation of the tentative packing model of the β-phase, with the unit cell shown. Peripheral side chains have been omitted. The main symmetry directions of graphite are indicated in red.

further understand the direct translation of the solution behavior to the surface layers upon solution deposition, the work discussed in the following sections explored the self-assembly of **1** at the liquid−solid interface and on the surface.

Self-Assembly at the Liquid−Solid Interface. In order to investigate the effects of substituents on lateral interactions at the molecular level, the organization of **1** at a liquid−solid interface was studied with scanning tunneling microscopy (STM). Alkylated HBCs and other HBC derivatives have been studied at the liquid−solid interface and shown to form two-dimensional arrays of monolayers. However, it should be taken into account that the outcome of the self-assembly process is the result of intermolecular interactions, including molecule−substrate, molecule−solvent, and solvent−substrate interactions. Different surface-confined supramolecular patterns are formed depending on the nature of the alkyl chains (linear, branched, etc.), as shown by STM with molecular and even submolecular resolution.[75] This raises the question of what influence the substituents of the HBCs **1** have on the structure of the surface-confined HBC networks.

Figure 3a displays an STM height image of a monolayer of **1b** recorded at the phenyloctane−highly oriented pyrolytic graphite (HOPG) interface shortly after deposition of a droplet of a phenyloctane solution if **1b** (5 × 10^{-4} M). Two domains with different orientations that are separated by a domain boundary can be recognized. Inside each domain, alternating rows of brighter and darker contrasts oriented along one of the three equivalent crystallographic axes of HOPG are visible. Each row is composed of regularly spaced bright spots that can be assigned to the aromatic part of the molecule. On the basis of both the assumption that the aromatic part of **1b** favors heteroepitaxial growth with respect to the underlying HOPG surface and the "triangular" appearance of the aromatic parts in high-resolution images (Figure 3b), a molecular packing model of the α-phase is suggested (Figure 3c). The orientation of the peripheral side chains cannot be deduced from the STM contrast. This is in agreement with previous observations of self-assembled monolayers of HBCs and is attributed to the high conformational mobility of the side chains.[76] On the basis of the size of the areas not being occupied by the aromatic parts and the known periodicity of densely packed alkanes on HOPG (∼0.43 nm),[77,78] there is enough space for all of the side chains to be adsorbed. Notably, the contrasts of the aromatic moieties of adjacent rows are alternating. It has been previously observed for different HBC derivatives that the contrast (brightness) of the HBC units within a single domain can regularly or randomly vary as a result of different positions of the molecules in the tip−substrate gap.[76] A unit cell of **1b** at the phenyloctane−HOPG interface contains two molecules; the cell parameters are a = 4.7 ± 0.2 nm, b = 2.9 ± 0.1 nm, and γ = 81 ± 5°, and the area occupied by the unit cell is 13.3 ± 0.9 nm^2.

During the course of the measurements, another type of crystallographic domain (β-phase) started to appear (Figure 3d). The β-phase domains consist of rows of molecules with the same STM contrast. However, these rows are not oriented along one of the three equivalent crystallographic axes of the underlying graphite. Instead, they are tilted by an angle of 22 ± 2°. High-resolution images suggest that each row is composed of dimers of molecules with opposite orientations (Figure 3e). A unit cell of the β-phase-type domains consists of two molecules;

(75) De Feyter, S.; De Schryver, F. C. *Chem. Soc. Rev.* **2003**, *32*, 139–150.
(76) Samori, P.; Fechtenkotter, A.; Jackel, F.; Bohme, T.; Müllen, K.; Rabe, J. P. *J. Am. Chem. Soc.* **2001**, *123*, 11462–11467.
(77) Rabe, J. P.; Buchholz, S. *Science* **1991**, *253*, 424–427.
(78) McGonigal, G. C.; Bernhardt, R. H.; Thomson, D. J. *Appl. Phys. Lett.* **1990**, *57*, 28–30.

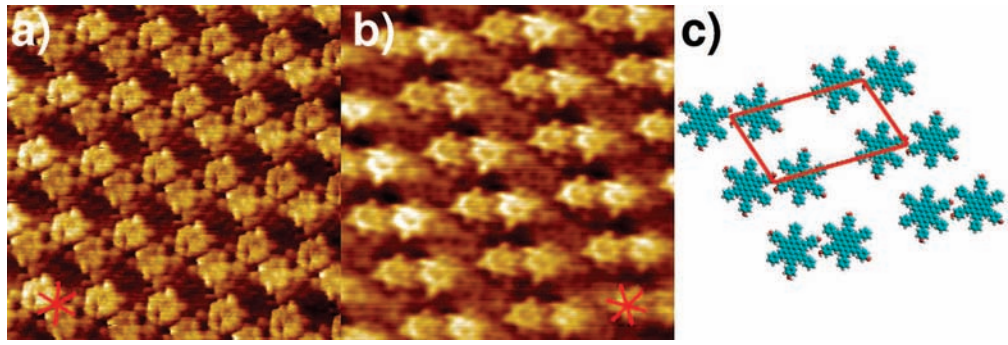

Figure 4. (a) High-resolution STM image of **1b** at the TCB−graphite interface (16.2 × 16.2 nm^2, i_T = 20 pA, V_S = −456 mV, 5161 TCB). (b) High-resolution STM image of **1c** at the TCB−graphite interface (inverse Fourier transform) (17.1 × 17.1 nm^2, i_T = 58 pA, V_S = −509 mV). (c) Schematic representation of the tentative packing model for **1c** at the TCB−graphite interface, with the unit cell shown. Peripheral side chains have been omitted. The main symmetry directions of graphite are indicated in red.

the unit cell parameters are $a = 3.1 \pm 0.1$ nm, $b = 2.9 \pm 0.1$ nm, and $\gamma = 76 \pm 4°$, and the area occupied by the unit cell is only 8.8 ± 0.7 nm^2. The orientation of the peripheral side chains cannot be conclusively determined. However, there is only space for two of the six side chains to be adsorbed on the surface. In addition to the β-phase, Figure 3d shows an α-phase domain. However, this domain contains linear defects that can be ascribed to the emergence of the β-phase. On the time scale of the measurements (5−28 h), a full transition from the α-phase to the β-phase was not observed.

Figure 4a shows a high-resolution STM image of **1b** at the interface of 1,2,4-trichlorobenzene (TCB) and HOPG. The molecular packing resembles the β-phase packing of **1b** in phenyloctane. The unit cell parameters in TCB also are comparable ($a = 3.2 \pm 0.1$ nm, $b = 2.9 \pm 0.2$ nm, $\gamma = 74 \pm 5°$), and the area occupied by the unit cell is 9.3 ± 0.8 nm^2. Domains similar to the α-phase in phenyloctane were not observed.

Various attempts to visualize **1c** at the interface of phenyloctane and HOPG failed. Deposition of **1c** from a TCB solution (5×10^{-4} M) on graphite resulted in the formation of domains with α-phase-type packing (Figure 4b). The unit cell parameters of the α-phase of **1c** in TCB are $a = 4.9 \pm 0.2$ nm, $b = 3.1 \pm 0.2$ nm, and $\gamma = 80 \pm 4°$, and the area occupied by the unit cell is 15.2 ± 1.0 nm^2. A tentative molecular packing model is depicted in Figure 4c.

From a comparison of the unit cells, it becomes obvious that the structural evolution of monolayers of **1b** at the phenyloctane−graphite interface is directed toward a higher packing density. Phase transitions of HBCs decorated by *n*-pentacontane have been observed previously.[79] A general notion is that molecular packing before the phase transition is kinetically favored, whereas packing after the phase transition is thermodynamically more stable. In case of the α-phase, where the rows of molecules are oriented along one of three main crystallographic axes of graphite, heteroepitaxial growth is kinetically favored. The dense packing in the case of the β-phase, however, allows a greater enthalpy gain. Because of the lack of information on the position of the side chains, it is difficult to evaluate their importance in the phase transition. As the density of packing increases, areas that are not occupied by aromatic cores decrease, and four out of the six side chains become desorbed from the surface (provided that there is always a maximum possible number of the side chains adsorbed). Since a graphite surface is hydrophobic, we can reasonably assume that the hydrophilic side chains desorb preferentially. Using a more polar solvent such as TCB might thus favor the formation of the β-phase by decreasing the energy barrier for the phase transition and stabilizing the β-phase. This is consistent with the observation of monolayers of **1b** at the TCB−graphite interface, where only the β-phase-type packing is observed. On the other hand, **1c** forms exclusively α-phase-type domains at the TCB−graphite interface. This is probably due to steric effects, which do not favor formation of β-phase domains.

With the assumption that the side chains cannot be visualized because of their high mobility (see above), the β-phase, which is favored in the more polar solvent (TCB) and can be observed only for **1b**, displays a higher degree of order (as a greater area of the surface is occupied by well-ordered aromatic units). As the α-phase is the only type of packing observed for **1c**, it can then be considered as less ordered. Various attempts to visualize **1a** at TCB−HOPG and phenyloctane−HOPG interfaces were made, but no evidence of adsorption of **1a** on the substrate was acquired, presumably because of the branched character of the alkyl chains, which weakens the interactions with the substrate. Therefore, the different degrees of ordering for **1** arising from the different bulkiness of substituents are consistent with the observed LC behavior and self-assembly in solution (see above).

Self-Assembly and Fiber Formation on Surfaces. In addition to the information regarding the self-assembly of HBC molecules in solution and at the liquid−solid interface, the deposition of molecular aggregates from a suitable solution onto the substrate is important for their implementation in electronic devices. Other factors, such as the solvent evaporation rate and interactions with the surface, may govern this process. To further understand the relation between structure formation on the surface and self-assembly in solution, the same cosolvent solution of **1** as described above was deposited by drop-casting onto the surface. The formed structure was then investigated using scanning electron microscopy (SEM) and transmission electron microscopy (TEM).

First, the 2:1 MeOH/$CHCl_3$ solution of **1b** was drop-cast onto a silicon wafer at room temperature, and the solvent was then allowed to evaporate. Inspection by SEM (Figure 5a) revealed long fibers with diameters between 200 and 500 nm and lengths of several tens of micrometers. Remarkably, at places where the fibers were densely packed, a coiled organization was observed. Inview of the nonchirality of **1b**, the formed helical

(79) Piot, L.; Marchenko, A.; Wu, J. S.; Müllen, K.; Fichou, D. *J. Am. Chem. Soc.* **2005**, *127*, 16245–16250.

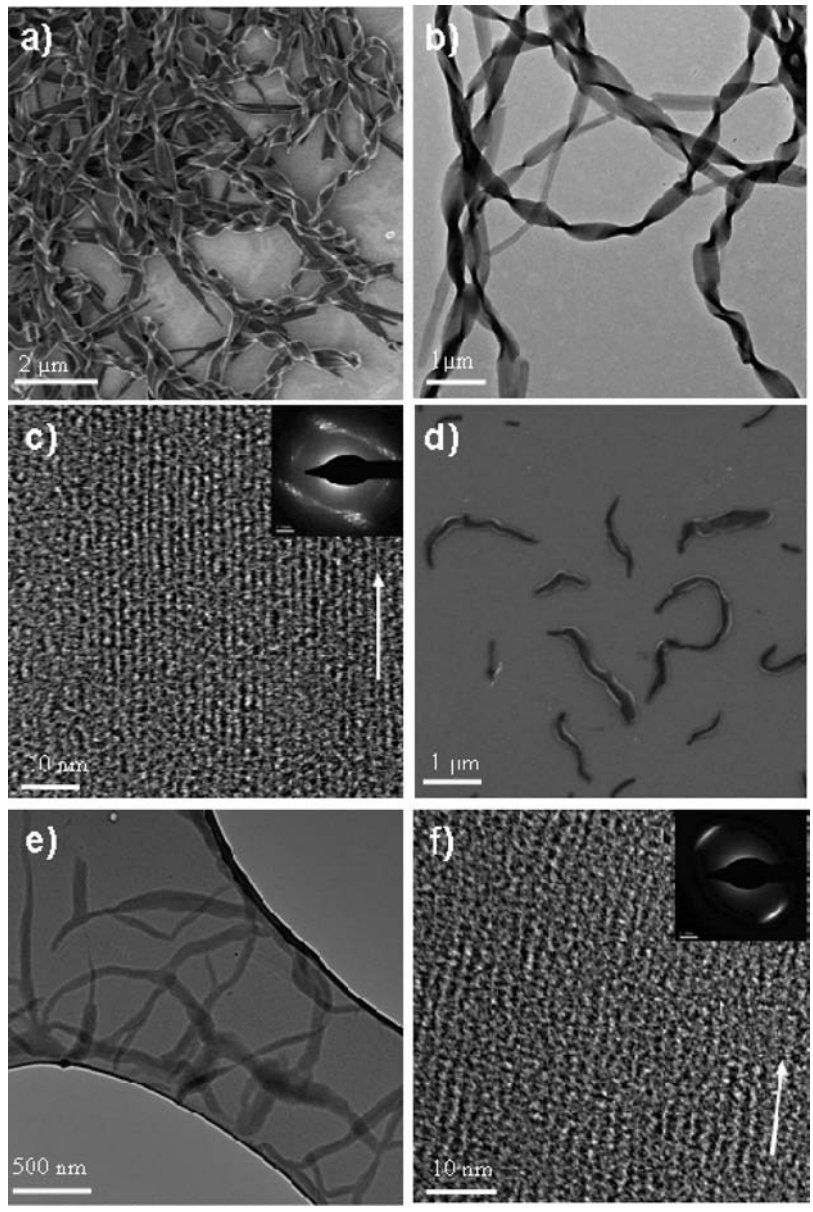

Figure 5. (a) SEM and (b) TEM of **1b** grown from 2:1 MeOH/$CHCl_3$ solution. (c) HRTEM image displaying columnar structures of **1b** (inset: ED pattern with reflections assigned to the π-stacking distance of 0.35 nm). (d) SEM and (e) TEM of **1c** grown from 2:1 MeOH/$CHCl_3$ solution. (f) HRTEM image displaying columnar structures of **1c** (inset: ED pattern with reflections assigned to the π-stacking distance of 0.35 nm).

superstructure could be ascribed to the tilted packing of disk molecules along the columns. This phenomenon of the formation of coiled tubular superstructures was previously reported for nonchiral amphiphilic discotics.[15,49] The stacking of many fibers suggested that they were already formed in solution. Additionally, the fibers were distributed randomly over the substrate, implying that spinodal dewetting did not significantly influence the deposition of the aggregates, presumably as a result of the limited mobility of large aggregated species on the thin film.[54] On the basis of the molecular size, the submicron-sized structures consisted of ~100−250 bundles of self-assembled columnar superstructures of **1b**. These results impressively confirmed the strong aggregation and π-stacking tendency of **1b**, allowing the growth of fibrous superstructures on the substrate. TEM characterization on carbon-film-covered Cu grids showed identical coiled fibrous superstructures (Figure 5b). High-resolution TEM (HRTEM) images displayed individual columns along the fiber direction with a pronounced columnar orientation (Figure 5c), suggesting a high supramolecular order. The electron diffraction (ED) pattern of these fibers (Figure 5c, inset) exhibited a pattern characteristic of the crystalline state, confirming the high degree of order in the fibrous structures. The ED pattern additionally indicated a tilting of disk molecules toward the columnar axis, with a corresponding intracolumnar period of 0.40 nm and π-stacking distance of 0.34 nm. This was also in agreement with the bulk organization observed by X-ray analysis.

The structure formation on the surface of **1a**, however, was found to be strongly concentration-dependent. Below a concentration of 5.0×10^{-5} M, no fibrous structures were formed, even at MeOH/$CHCl_3$ ratios of up to 2:1. Instead, only small globular droplets composed of randomly deposited material were observed (Figure S4c,d in the Supporting Information). This corresponded to the low aggregation behavior of **1a** in solution, as demonstrated by the UV and PL spectra (Figure S2 in the Supporting Information).

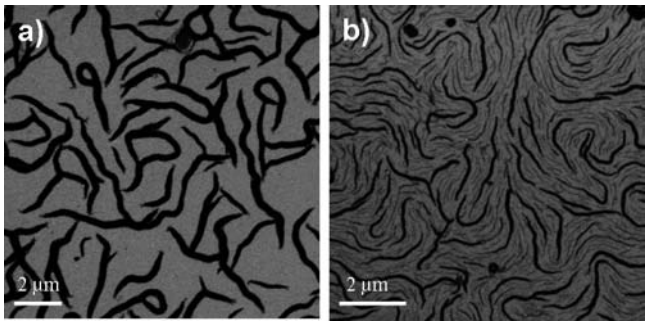

Figure 6. SEM images of **1a** from (a) 2:1 MeOH/$CHCl_3$ solution (1.0×10^{-4} M) and (b) 2:1 MeOH/CH_2Cl_2 solution (1.0×10^{-5} M).

Surprisingly, however, when the concentration was increased to 1.0×10^{-4} M, at which the UV−vis and PL spectra still did not indicate any aggregates in solution (not shown), micrometer-long fibers were formed on the surface after solvent evaporation (Figure 6a). Accordingly, this concentration dependence suggested that fiber formation would only occur if the concentration of **1a** in a thin film was subjected to spinodal dewetting at a certain thickness,[54,80,81] where the molecules start to self-assemble. In order to further verify the role of the solvent evaporation on the self-assembly of **1a** on the surface, $CHCl_3$ was replaced by the low-boiling-point solvent CH_2Cl_2. Interestingly, in the case of 2:1 MeOH/CH_2Cl_2, a high concentration was not crucial, since dispersed and oriented fibrous nanostructures were observed even at low concentration (1.0×10^{-5} M) (Figure 6b). It was assumed that the critical concentration for the spinodal dewetting was more easily achieved because of the rapid evaporation of CH_2Cl_2.

Although **1c** also showed pronounced aggregation stability in solution, the fiber morphology on the surface after drop-casting from 2:1 MeOH/$CHCl_3$ (1.0×10^{-5} M) was in fact different from that for **1b**. As depicted in Figure 5d,e, only short fibrous or rodlike nanostructures with lengths between 500 nm and 5 μm were formed, indicating the poorer tendency for self-assembly of **1c** than of **1b**. This was in accordance with the UV−vis and PL results in solution (2:1 MeOH/$CHCl_3$), where **1b** (Figure 2) showed distinctly red-shifted bands as compared with **1c** (Figure S3 in the Supporting Information). Obviously, the lower aggregation tendency of **1c** could be ascribed to the steric bulkiness of additional phenyl groups suppressing the intermolecular π interactions, which was also responsible for the LC behavior in the solid state. Nevertheless, HRTEM images (Figure 5f) revealed individual columns along the direction with well-oriented columns for **1c**. The ED pattern (Figure 5f, inset) indicated the typical LC state in the fibrous structures with the typical π-stacking distance of 0.35 nm, which is also in agreement with the X-ray measurements in the bulk.

To finally summarize all of the results for the control of self-assembly in the bulk, solution, at the liquid−solid interface, and on the surface, the bulk organization of **1** was strongly dependent on the steric demand of the alkyl substituents. The X-ray scattering studies indicated that substitution with linear alkyl chains (**1b**) led to a pronounced intermolecular interaction and thus a high crystallinity at low temperature, whereas the introduction of bulky branched alkyl chains (**1a**) and alkylphenyl substituents (**1c**) decreased the intermolecular interactions and induced an LC phase over the whole temperature range measured. The incorporation of hydrophilic and hydrophobic substituents at the periphery of the core allowed the study of the self-assembly in the polar/apolar environment of the cosolvent system MeOH/$CHCl_3$. Similar to the bulk organization, compound **1b** revealed strong aggregation in solution, as implied by the large bathochromic shift of the main bands in the UV−vis and PL spectra. Additional temperature-dependent UV−vis and PL measurements revealed a reversible aggregation and dissociation process. In contrast, compound **1a** did not show such pronounced aggregation, even at high methanol concentration, because of the attached branched alkyl chains, which hindered an intermolecular approach of the molecules in solution and thus increased the solubility. Interestingly, **1c** exhibited remarkably higher stability of the aggregates, which did not disassemble even at 70 °C. This result demonstrated that the stability of π-stacked aggregates can be greatly enhanced by using a hexaphenyl-substituted HBC scaffold in which the possible intermolecular interlocking of peripheral phenyl groups is present.

The same tendencies were observed for self-assembled monolayers of **1** at the liquid−HOPG interface. Substitution by linear alkyl chains (**1b**) led to high crystallinity, which was concomitant with the phase transition from α-phase to ordered β-phase at the phenyloctane−graphite interface. For steric reasons, **1c** was visualized only as the α-phase at the more polar TCB−HOPG interface, whereas the substitution with branched alkyl chains in **1a** led to poor adsorption on this substrate.

The aggregates of **1b** and **1c** formed in solution could be directly deposited on the substrate, and as expected, the high tendency of **1b** to self-assemble led to long helical fibers, whereas **1c** only showed short wormlike rods. The HRTEM images of the fibers displayed well-oriented columnar structures for **1b** and **1c**, indicating a high supramolecular order at the nanoscale. The ED patterns exhibited the characteristic crystalline and LC states for **1b** and **1c**, respectively, which were in agreement with the X-ray measurements in the bulk, further confirming the different degrees of order in the fibrous structures. Although **1a** showed poor self-assembly in solution, its structure formation on the surface was found to be strongly concentration-dependent. This could be ascribed to the critical concentration for spinodal dewetting, which was more easily achieved when a high concentration of **1a** or the low-boiling-point solvent CH_2Cl_2 was used, resulting in dispersed fibrous nanostructures on the surface.

Conclusions

Organization and order of discotic nanographenes as organic semiconductors are exceptionally important for their performance in electronic devices. For these applications, the candidate molecules are processed by deposition from solution on a surface. The present results elucidate the important relationship among self-organization in the bulk, the propensity for self-assembly in solution and at a liquid−solid interface, and formation of fibrous nanostructures on the surface. Three crucial factors that control the thermotropic properties and self-assembly in solution and on surfaces have been identified: the steric demand of alkyl and alkylphenyl substituents; noncovalent hydrophilic−hydrophobic interactions of the substituents; and processing conditions. Accordingly, this work provides a

(80) Muller-Buschbaum, P.; Gutmann, J. S.; Lorenz-Haas, C.; Wunnicke, O.; Stamm, M.; Petry, W. *Macromolecules* **2002**, *35*, 2017–2023.
(81) Higgins, A. M.; Jones, R. A. L. *Nature* **2000**, *404*, 476–478.

comprehensive overview of the supramolecular behavior of new discotic nanographene materials.

Acknowledgment. This work was financially supported by the Max Planck Society through the program ENERCHEM, the German Science Foundation (Korean−German IRTG), and DFG Priority Program SPP 1355. We thank Dr. Nicole Kirsch for assistance in the preparation of the manuscript.

Supporting Information Available: Experimental procedures and analytical data, ^{1}H NMR spectra of **1c**, UV−vis and photoluminescence spectra of **1a** and **1c**, and SEM images of **1a**−**c**. This material is available free of charge via the Internet at http://pubs.acs.org.

JA808979T